Areal density effects on the blocking of 3-keV Ne^{7+} ions guided through nanocapillaries in polymers

N. Stolterfoht and R. Hellhammer
Helmholtzzentrum Berlin für Materialien und Energie, D-14109 Berlin, Germany

B. Sulik and Z. Juhász
Institute of Nuclear Research (ATOMKI), 4001 Debrecen, Hungary

V. Bayer and C. Trautmann
GSI Helmholtzzentrum für Schwerionenforschung, D-64291 Darmstadt, Germany

E. Bodewits, G. Reitsma, and R. Hoekstra
KVI Atomic Physics, University of Groningen, 9747 AA Groningen, The Netherlands
(Received 4 June 2013; published 30 September 2013)

We studied blocking effects on ion guiding through nanocapillaries in highly insulating polyethylene terephthalate (PET). The experiments were initiated in view of a previous study with capillaries in polycarbonate (PC) for which strong blocking effects were observed, whereas for PET these effects could not be detected. The aim was to find out whether the different results are caused by differences in the PET and PC materials or by differences in the areal densities of the capillaries. Transmission experiments of 3-keV Ne^{7+} ions were performed for a variety of PET samples with an areal capillary density ranging from 3 to 60×10^6 cm^{-2}. The tilt angles were close to zero degree because previous blocking effects were found to be largest at small angles. Our results clearly show that blocking effects also exist for PET and that they are sensitively dependent on the areal capillary density, i.e., the mean capillary distance. The potential produced by the charges accumulated in neighboring capillaries is calculated showing that it plays an important role in the ion blocking. In addition, model calculations are performed providing expressions to determine the direct ion transmission for small tilt angles and divergent ion beams.

DOI: 10.1103/PhysRevA.88.032902 PACS number(s): 61.85.+p, 34.50.Fa, 32.80.Fb

I. INTRODUCTION

In recent years the guiding of highly charged ions in capillaries with diameters of a few hundred nanometers has received considerable attention. Capillaries in highly insulating materials like polymers accumulate ions at the wall so that charge patches are created. Sufficient charge collection produces a repulsive electric field, which results in the deflection of subsequently passing ions. The deflection occurs at relatively large distances to the capillary wall so that electron capture into the projectile is inhibited. Thus, the ions are guided along the capillary axis maintaining their incident charge state during their passage even when the capillary axis is tilted with respect to the incident beam direction. The essential property of the ion guiding is the self-organizing process, which governs the charge deposition inside the capillaries [1].

Initial studies of ion guiding phenomena in insulating materials were performed using capillaries in polyethylene terephthalate (PET) [1–3]. During past years the interest in this field increased and several laboratories performed experiments using different materials such as PET [4–9], polycarbonate (PC) [10], SiO_2 [11], and Al_2O_3 [12–14]. Moreover, electrons were used as projectiles guided through capillaries in Al_2O_3 [15,16] and PET [17,18].

In addition to multitude capillaries, guiding of highly charged ions were studied between flat glass plates [19] and in single capillaries with constant diameter [20,21]. In addition, single capillaries in tapered geometry were applied with the intention to produce submicrometer sized beams [22,23]. In a recent investigation the temperature of a single capillary was varied to control the influence of the surface conductivity [24]. Apart from the experimental work, a series of theoretical studies [25–29] has provided detailed information about the guiding mechanisms.

In previous experiments particular attention has been given to the dynamic properties of the ion fraction guided through the capillary [30–33]. Due to the formation of the entrance charge patch, the ion transmission starts delayed after a certain threshold and rises to a maximum where stationary (equilibrium) conditions are expected to be reached and maintained. Commonly one considers the system in equilibrium when the fraction of transmitted ions remains constant after reaching a maximum transmission. For instance, stationary conditions have always been observed in ion transmission experiments performed with PET. Only recently, experiments with PC capillaries have shown that after reaching a maximum the transmitted ion fraction decreases with increasing charge insertion [34]. This observation has been referred to as a blocking effect on the ion transmission.

In the previous study [34] it has been confirmed that the blocking effects are absent for PET capillaries even for a considerable amount of inserted charges. It should be noted, however, that the number of capillaries per unit area in PET was an order-of-magnitude smaller than in PC. (Throughout this work the number of capillaries per unit area will be referred to as areal capillary density or simply as capillary density.) The areal density of the PET capillaries was 6×10^6 cm^{-2}, whereas it was from 1 to 5×10^8 cm^{-2} for PC capillaries [34]. Hence, the question arose whether the blocking effects are produced

by the difference in the PC and PET material properties or by the difference in the areal capillary densities. Note that the capillary density determines the mean distance of neighboring capillaries.

To address this question, it is useful to first consider further information from previous studies. For instance, it was found that the blocking effect in PC capillaries increases with decreasing tilt angle [34], i.e., the blocking effect maximizes for untilted capillaries. This finding is unexpected as the amount of charge deposited into the capillary increases with tilt angle. However, for nonzero tilt angle the charge is accumulated primarily in the entrance charge patch, whereas the charge deposited in the center of the capillary is relatively small [29]. It appears that the charge in the center of the capillary has an important effect on the ion blocking.

In recent simulations [28] it was concluded that the charge accumulated in a single capillary is not sufficient to create a repulsive field strong enough to reject the incident ions. This finding suggests that ion blocking is enhanced by the multitude of capillaries present in the neighborhood. Such collective neighbor effects were considered in simulations of ion guiding [25]. Experimentally, the neighbor effect is expected to be enhanced, when the distance to the capillary neighbors is reduced by increasing their areal density.

In the present work, we investigate the fraction of transmitted ions for capillary densities varying by more than one order of magnitude. The experiments are performed with PET capillaries to find out whether blocking effects exist also for this material. The data are acquired for tilt angles close to zero degree, since the blocking is largest for untilted capillaries. The experiments confirm that the blocking effect is strongly influenced by the mean distance of the capillaries. The ion blocking is attributed to the collective field produced by the charge accumulation in neighbor capillaries.

II. EXPERIMENTAL METHOD

The experiments were performed in an ultrahigh vacuum chamber mounted at the 14-GHz electron cyclotron resonance (ECR) ion source of the distributed LEIF-Infrastructure ZERNIKE-LEIF at KVI Groningen (Netherlands) [35]. The experimental method has been described in detail before [32] so that only a few details are pointed out here. The vacuum chamber was used in a high-vacuum mode, i.e., the base pressure was a few 10^{-8} mbar. The apparatus was set on high voltage to allow for the deceleration of the incident Ne^{7+} ions from 49 keV down to 3 keV. The ion current was varied within the range from 10 to 3000 pA. The beam was collimated to a diameter of 1.3 ± 0.2 mm with a divergence of about $\pm 0.25^\circ$.

Cylindrical parallel oriented capillaries were prepared by irradiating 10 ± 1 μm PET foils with 2.2-GeV gold ions at the GSI Helmholtzzentrum in Darmstadt [36]. The applied ion fluence was varied by a factor of 20 between 3×10^6 and 6×10^7 ions/cm^2. The irradiated foils were etched in 6N NaOH, converting each ion track into a cylindrical capillary. The duration of the etching was controlled such that the diameter of the capillaries was 140 ± 15 nm. A gold layer was evaporated in four directions under 30° on the front and the back sides of the PET foils forming a film of ~20-nm thickness to avoid a macroscopic charge

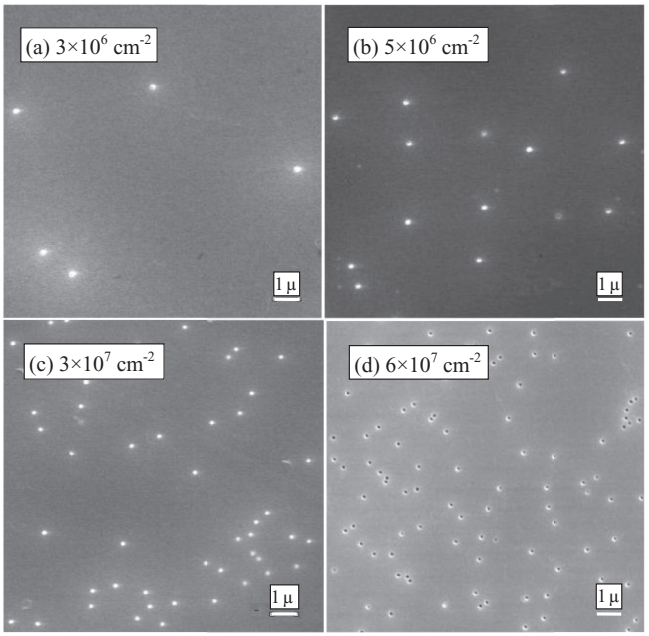

FIG. 1. SEM images of sample surfaces showing the capillaries used in the present experiments. The number given in each panel is the capillary density as also listed in Table I.

up mainly at the sample front surfaces. Figure 1 presents images obtained with scanning electron microscopy (SEM) to show the areal density δ_c of the capillaries. Due to the stochastic nature of the ion beam the capillary entries are statistically distributed over the surface. The densities and mean distances of the PET capillaries are summarized in Table I.

The capillary foils were mounted at a goniometer, which allowed for tilting the capillaries relative to the incident beam in two directions specified by the angles ψ and φ. The tilt angle ψ is an important parameter in the present study. The azimuthal angle φ was kept constant after its zero value was fixed using a laser for alignment. The PET target foils were spanned into circular frames with an inner diameter of 7 mm. By shifting the frame with the goniometer, the incident Ne^{7+} ion beam could be positioned at different spots within the target area. Hence, the results described below were obtained with unirradiated capillaries if not otherwise stated.

The neon ions emerging from the capillaries were analyzed with respect to their charge state, energy, and emission angle using an electrostatic 180° spectrometer, which could be rotated by an angle θ in the same plane as the tilt angle ψ. In the experiments the angular distribution of the transmitted

TABLE I. Areal density δ_c and mean distance l_c of the PET capillaries used in this work. For all samples the capillary diameter is 140 nm and the length is 10 μm.

Sample	δ_c (cm^{-2})	l_c (μm)
a	3×10^6	6
b	5×10^6	4.5
c	3×10^7	2
d	6×10^7	1

Ne^{7+} ions was measured for tilt angles near 0°. The angular resolution of the analyzer was 0.2° full width at half maximum (FWHM). For the direct incident beam (without the capillary target) a Gaussian-like angular profile with a FWHM of 0.5° was acquired. This width is expected to be a composition of the beam diameter, its divergence, and the angular resolution of the analyzer.

III. EXPERIMENTAL RESULTS

A. Transmission profiles

In the following, we present transmission profiles of 3-keV Ne^{7+} ions, whose incident charge state was preserved during the passage through the capillary. A transmission profile represents an angular distribution $dY(\theta,\phi)/d\Omega$ of Ne^{7+} ions transmitted through the capillaries as a function of the observation (or emission) angle θ. We recall that $\phi = 0°$ was fixed in the experiments. Figure 2 shows a series of selected transmission profiles for the tilt angles of $\psi \approx 0°$. The columns from left to right show profiles obtained with increasing capillary density (values given in the upper panels).

Each transmission profile is normalized to an integral current of $Q_d = 1$ nC, where Q_d is the total charge deposited by the beam on the front surface of the target foil. For a given incident beam current the deposited charge is a measure of time. Each graph indicates the charge Q_d collected until the instant when the profile is measured. Hence, the results in a given column represent the temporal evolution of the transmission profile for the corresponding capillary density.

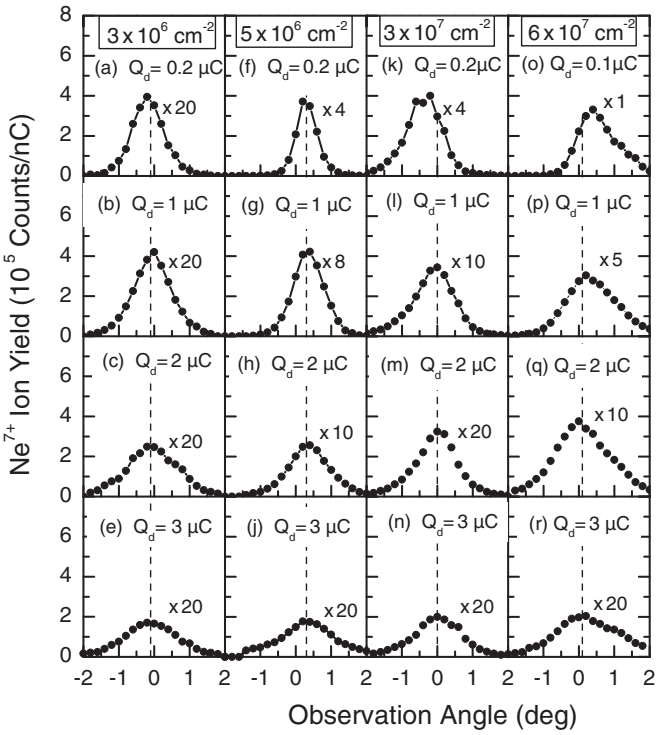

FIG. 2. Transmission profiles for 3-keV Ne^{7+} ions passing through capillaries in PET. The number given at the top of each column is the density of the capillaries. The parameter Q_d is the charge deposited by the incident beam at the front of the capillary sample.

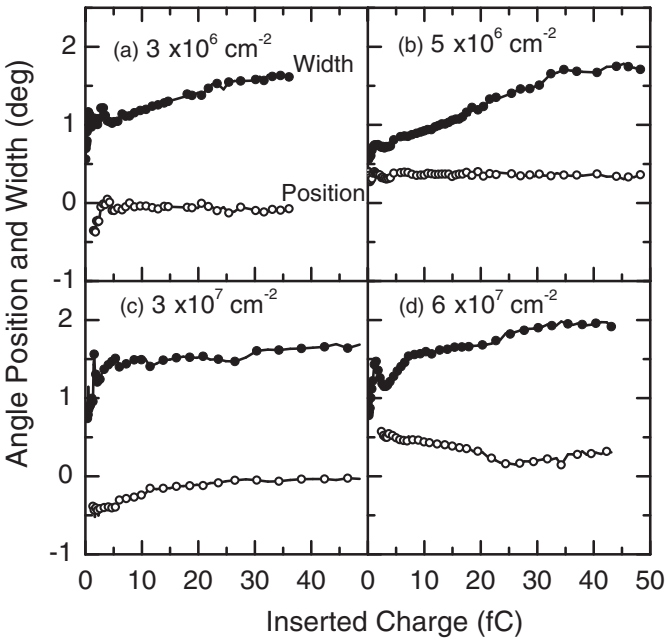

FIG. 3. Position (open circles) and width (full circles) of the transmission profiles shown in Fig. 2. The data are plotted as a function of the charge Q_{in} inserted into a single capillary. The density of the capillaries is given in each graph.

From Fig. 2 it is seen that the peak position of the transmission profiles is rather constant with increasing charge deposition, i.e., there are only small deviations of the profile position from the center value represented by the vertical dashed line. In Fig. 3 the peak positions are shown as open circles representing the mean emission angle obtained by numerical integration $\bar{\theta} = \int \theta\,(dY/d\Omega)d\theta / \int (dY/d\Omega)d\theta$ [32]. The data are plotted as a function of the charge Q_{in} inserted into a single capillary, which will be used in the following instead of the deposited charge Q_d (Fig. 2). The charges Q_{in} and Q_d are related by $Q_{in} = Q_d(d/D)^2$ where d is the diameter of the capillary (140 nm) and D is the diameter of the ion beam (1.3 mm). More information about the integration procedure and the charge conversion is given in a recent study [37].

From Fig. 3 it is seen that the mean emission angle changes slightly when the charge insertion increases. The variation of the mean angle reveals the formation of transient charge patches as has been discussed in detail previously [30–33]. Transient charge patches can be produced when the tilt angle deviates from zero. It should be pointed out that due to experimental uncertainties, it is difficult to set the capillary tilt angle exactly to zero. The tilt angle can only accurately be determined by the analysis of the data after the experiment. The actual tilt angle can be observed after sufficient charge is inserted into the capillary (i.e., asymptotically after reaching equilibrium conditions) since asymptotically the transient charge patches have essentially disappeared. In Fig. 2 the asymptotic peak positions vary within ±0.3°, which may be considered as the experimental uncertainty of setting the capillary at a given tilt angle.

Moreover, from the experimental analysis the full width at half maximum σ_θ of the transmission profiles can be

determined. In Fig. 3 the profile widths are plotted as curves represented by full circles. The curves show that widths are first increasing with increasing charge insertion and approach stable values for further charge insertion. We note that for the present tilt angles close to 0° the width σ_θ varies between 1° and 2° which is smaller than the width observed for nonzero tilt angles, as summarized in previous scaling laws [6]. Also, it is noted that the width of the profiles essentially does not change when the areal density of the capillaries is varied.

Diverse effects are responsible for the width of the transmission profiles, which have been discussed previously [6,25]. One may suppose that the nonparallelism of the capillaries produces the dominant contribution to the width of the emission profiles. However, this supposition is incorrect since under guiding conditions the nonparallelism results in a width independent of the charge state and energy of the projectile, which is clearly against experimental observations [6].

Returning to Fig. 2 we note that the transmission profiles vary in intensity when the charge deposition increases. Each profile is multiplied by a factor, which reveals its intensity variation. In the first column the multiplication factor is always 20 indicating that the profile intensity is essentially constant. However, in the last column the multiplication factor changes from 1 to 20 indicating a significant intensity loss with increasing charge deposition. This loss of intensity is a signature for the ion blocking [34]. Hence, we may conclude that blocking effects also exist for capillaries in PET so that there is no principle difference between the capillaries in PET and PC.

B. Recovery of the ion transmission

In the following, we address the question whether the loss of the ion transmission is transient or permanent. In principle the loss of transmission could be permanent due to fundamental material changes in the capillary interior. Thus, we consider the total ion yield Y_t transmitted through the capillaries, which is obtained from the integration of the transmission profiles,

$$Y_t = \int \frac{dY(\theta,\phi)}{d\Omega}\, d\Omega. \tag{1}$$

Since in this work only the ion yield with respect to the angle θ was measured, the integration over the angle ϕ was performed assuming that its dependence is described by a Gaussian function. The width σ_ϕ of the Gaussian was set to be equal to the width σ_θ of the transmission profile obtained for sufficiently large charge deposition. Then, the total yield was obtained by numerical integration of the experimental data.

As mentioned, we may consider the possibility that the loss of transmission is permanent. The ions could be blocked by an enhanced collection of charges inserted into the capillaries. In the case that the deposited charges retain a certain mobility, it is expected that after some time the charges are removed and the capillaries become again transparent. On the other hand, it may be possible that due to specific material properties the capillaries remain charged so that they permanently inhibit the passage of the ions.

To find an answer to these questions, the ion transmission at a fresh spot on the capillary sample was repeated after a 15 hours pause with the same capillaries as used before. After this pause it is expected that the majority of mobile charges are removed from the capillary interior. The measurements were performed with the highest available capillary density of 6×10^7 cm^{-2} (Table I) to enhance the blocking effect.

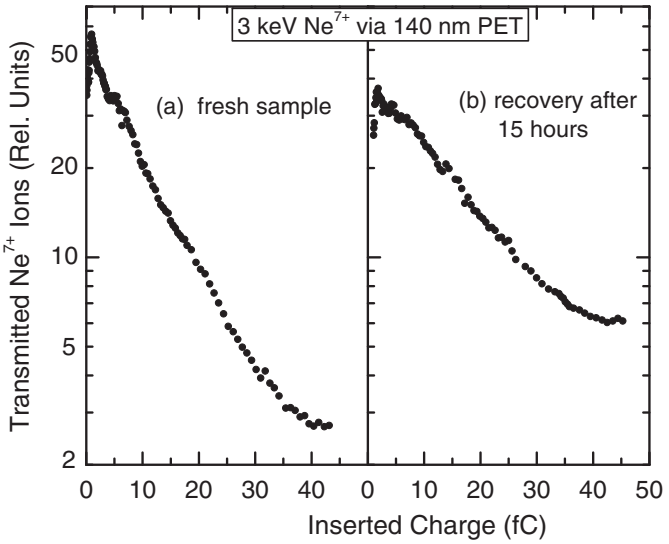

FIG. 4. Recovery of the capillary transmission after a 15 hour pause. The data were measured using 3-keV Ne^{7+} ions transmitted through PET capillaries with a density of 6×10^7 cm^{-2}. In (a) the ion transmission for a fresh spot on the capillary sample is shown. In (b) the repetition of the experiments at the same spot is presented. The data are plotted as a function of the inserted charge Q_{in}.

In Fig. 4 the total intensity of the transmitted ions is plotted as a function of the inserted charge Q_{in}. Figures 4(a) and 4(b) show the results obtained with the fresh and used capillaries, respectively. (We recall that the transmission profiles associated with the fresh capillary measurement are shown in the last columns of Fig. 2.) For the fresh capillaries the ion intensity rises initially very rapidly to a maximum from where it drops continuously by more than an order of magnitude. The initial increase of the ion intensity is expected to be due to a guiding effect that compensates the intensity loss due to a small nonzero tilt angle. This intensity loss can be understood from Fig. 10(a) presented in the Appendix.

In Fig. 4(b) the repetition of the measurement shows the same qualitative behavior as the original experiment. After an initial rapid increase, the ion intensity decreases due to blocking effects. The similarity of the two curves in Figs. 4(a) and 4(b) indicates that the transmission properties of the capillaries are essentially recovered after the 15 hours pause. This shows that most of the charges within the capillary interior are removed. However, certain differences between the two curves persist revealing that some rest charge remained within the capillaries. Nevertheless, it may be concluded that the differences between PET and PC [34] are not caused by differences by the material properties. Thus, it is likely that the blocking is influenced by the capillary density. The role of the capillary density for the ion transmission will be analyzed next.

C. Capillary density effects on the ion blocking

In the following we study the temporal evolution of 3-keV Ne^{7+} ion transmission for different capillary densities. As before, the total ion yield Y_t was determined by integrating the transmission profile partially shown in Fig. 2. However, for a better comparison of the data obtained with different capillary densities, we normalized the total intensity of transmitted ions. In the following, we consider the fraction of transmitted ions obtained by dividing Y_t by the total number of ions Y_{in} incident into the multitude of capillaries involved:

$$f_t = \frac{Y_t}{Y_{\text{in}}}. \tag{2}$$

The number of incident ions $Y_{\text{in}} \propto \delta_c$ is proportional to the capillary density δ_c so that f_t contains a division by that density. We note that the quantities Y_t and Y_{in} were measured only on a relative scale so that the fraction f_t depends on a proportionality factor. However, the results for each capillary density involve the same proportionality factor, which will be determined below in comparison with the model calculations performed in the Appendix.

In Fig. 5 the results for the transmitted ion fraction are plotted as a function of the inserted charge. Each graph labeled (a)–(d) is associated with a certain capillary density in accordance with the notation in Table I. All curves exhibit a rapid increase at the beginning of the charge insertion, which can be attributed to small deviation from the 0° tilt angle as already discussed for the data in Fig. 5(d) in the preceding section. As mentioned, the guiding effect compensates the initial loss of the transmitted ions.

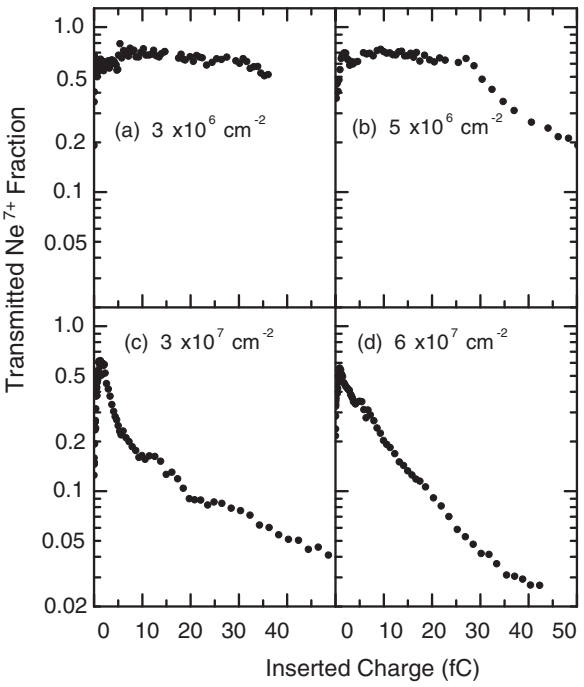

FIG. 5. Fraction f_t of 3-keV Ne^{7+} ions transmitted through capillaries in PET plotted as a function of the inserted charge. The tilt angle is close to 0°. The areal capillary density is given in each graph.

After the guiding has reached equilibrium, we expect that for small angles the transmitted ion fraction reaches a maximum, which is nearly unity. However, the divergence of the beam leads to some loss of ions within the capillaries. For the present divergence of ±0.25° the transmitted ion fraction was determined to be 0.7 as a result of calculations in the Appendix. Thus, the unknown proportionality factor involved in f_t was fixed by setting the maximum of the data in Fig. 5(a) equal to 0.7. Then, the curves for the other densities could be put on an absolute scale, too.

From Figs. 5(a) and 5(b) it is seen that the transmitted ion fraction for the lower densities of 3×10^6 and 5×10^6 cm^{-2} are rather constant, whereas the results in Figs. 5(c) and 5(d) for the higher densities of 3×10^7 and 6×10^7 cm^{-2} decrease strongly with the inserted charge. Hence, it is obvious that the observed blocking effects are much stronger for the high densities than for the low densities.

The strong decrease of the ion transmission can be understood in terms of a self-enhancing effect involved in the ion blocking process. Ion blocking is the result of a repelling field produced by the charge deposited in the capillary interior. This quantity will be denoted as an absorbed charge in the following. When the capillary density increases, the repelling field is enhanced by neighbor contributions. Then, the ion blocking is enhanced so that the charge absorbed within the capillaries increases, which in turn increases the repelling field and so on. Hence, we expect blocking effects beyond proportionality when the capillary density increases. The reason for the nearly instant inset of the ion blocking for the higher density capillary will be discussed in more details below in conjunction with model calculations.

The self-enhancing effect of the ion blocking can be revealed in more detail by means of the amount of charge Q_a absorbed in the capillary interior. This charge is obtained from the absorbed charge current,

$$J_a = J_{\text{in}} - J_t, \tag{3}$$

where J_{in} and J_t are the incident and transmitted current, respectively. The absorbed charge is deduced by the time integration,

$$Q_a(t) = \int_0^t J_a(t')\,dt', \tag{4}$$

which can be replaced by the integration over the incident charge using $t = Q_{\text{in}}/j_{\text{in}}$ (and $dt = dQ_{\text{in}}/j_{\text{in}}$),

$$Q_a(Q_{\text{in}}) = \int_0^{Q_{\text{in}}} f_a(Q'_{\text{in}})\,dQ'_{\text{in}}, \tag{5}$$

where we introduced the current fraction $f_a = J_a/J_{\text{in}} = 1 - f_t$ obtained from the transmitted fraction f_t given in Fig. 5.

The results of the integration are plotted in Fig. 6 where the absorbed charge Q_a is given as a function of the inserted charge Q_{in}. The figure shows four curves each of which is attributed to a density of the capillaries. For the two lower capillary densities (3×10^6 and 5×10^6 cm^{-2}) the absorbed charge amounts to about 30% of the inserted charge for values smaller than ~35 fC. However, for the higher capillary densities (3×10^7 and 6×10^7 cm^{-2}) the absorbed charge amounts to values as large as 80% of the inserted charge. This large value for the absorbed charge is the reason for the self-enhanced blocking

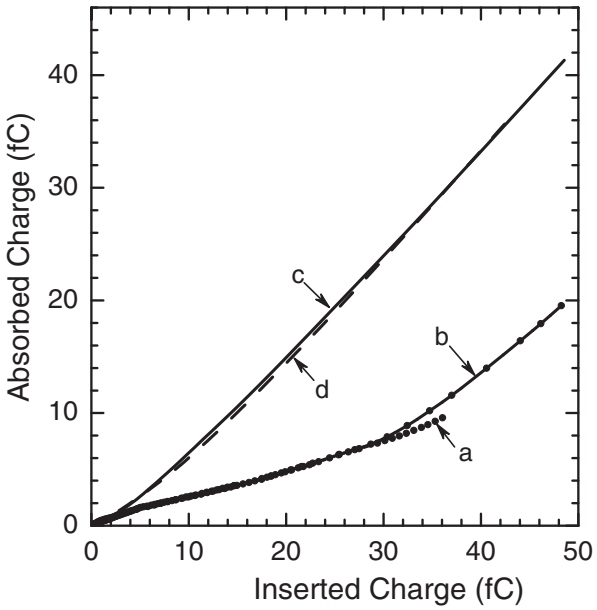

FIG. 6. Charge Q_a absorbed in a single capillary during the transmission of 3-keV Ne^{7+} ions as a function of the inserted charge Q_{in}. The results are obtained from the data in Fig. 5 using Eq. (5). The curves labeled a, b, c, and d correspond to the areal densities indicated in Fig. 5.

process. Indeed, this is likely due to the blocking effects observed in Figs. 5(c) and 5(d) which are much stronger than those found in Figs. 5(a) and 5(b).

It should be pointed out that the absorbed charge stays only transiently within the capillary. Electric fields, produced by the absorbed charges, transport these charges out of the capillary interior to the exits where they are finally depleted at the gold film covering the sample surfaces [28]. Therefore the absorbed charge splits into two components:

$$Q_a = Q_d + Q_c, \tag{6}$$

where Q_d is the charge depleted at the sample surface and Q_c is the collected charge remaining within the capillary. The electric field increases with increasing charge absorption so that the charge depletion increases, too. Therefore, the actual charge Q_c collected in the capillary is smaller than Q_a. The latter charge can be used as a reasonable estimate for the collected charge only in cases for which the charge transport is small. Otherwise, Q_a has to be used as an upper limit of the actual charge present in the capillary.

IV. ION BLOCKING BY NEIGHBOR CAPILLARIES

In this section we describe a model that estimates the potential produced by neighbor capillaries leading to a partial or full blocking of the inserted ions. To obtain the potential produced by all charges, their Coulomb potentials are summed as follows:

$$V(\mathbf{r}) = \sum_i \frac{q_i}{|\mathbf{r} - \mathbf{r}_i|} + \sum_n \sum_i \frac{q_{i,n}}{|\mathbf{r} + \mathbf{r}_{i,n}|} + \text{images}, \tag{7}$$

where the first and second term refer to the given capillary and neighbor capillaries, respectively. The index i runs over the charges in a single capillary and the index n runs over the number of neighbor capillaries. The number of capillary neighbors labeled n was limited to a finite value beyond which more capillaries could be added without a noticeable change of the potential.

Within the present model, capillaries are assumed to have a square opening with size a and length L. The square shape is chosen to achieve an analytic expression for the potential of a rectangular, homogeneously charged surface of the capillary interior. The summation over i in Eq. (7) is replaced by an integration, which can be solved analytically. The width of the opening is set to be $a = d\sqrt{\pi}/2$ so that the entrance areas of the square and circular openings are equal.

In Eq. (7) the term denoted images is added to account for the grounded metal layer evaporated on the front and back side of the PET foil (noted in the experimental Sec. II). The grounded metal layers are taken into account by adding a reasonable set of image charges (in fact, images of the charged surfaces) with alternating sign on both sides, using the metal layer as a mirror. More details will be presented in a future publication.

The replacement of the circular capillary by a square capillary is expected to be a reasonable approximation as the average distance between neighbor capillaries is significantly larger than the capillary diameter. Note that this simple model provides the potential inside a capillary due to an arrangement of charged rectangular surfaces in it, and a large ensemble of neighboring capillaries identically charged. However, it does not account for how these charge arrangements are created.

At the simplest arrangement, the deposited charge is assumed to be distributed homogeneously within the capillary. Moreover, only the upper and lower wall of the four capillary sides are covered by charges. The resulting potential for a

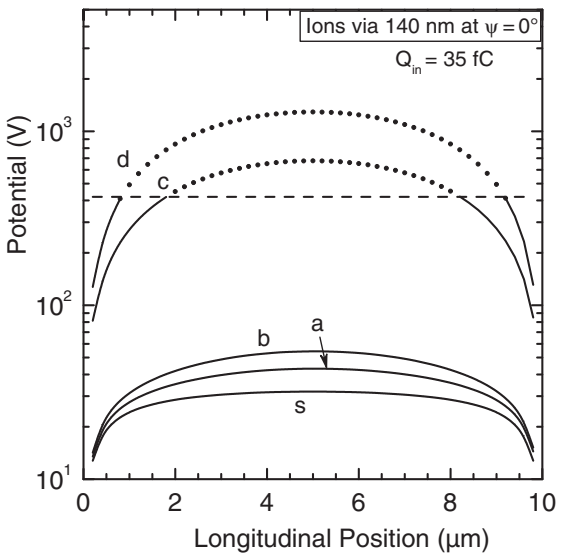

FIG. 7. Potential along the longitudinal axis in the center of the capillary. The curve labeled *s* refers to a single capillary. The curves labeled a, b, c, and d are obtained with capillary densities given in Table I. The inserted charge is 35 fC. The horizontal dashed line at 428 V indicates the potential barrier which cannot be passed by 3-keV Ne^{7+} ions. The dotted lines indicate that the potential cannot exceed the 428 V line.

single capillary is in reasonable agreement with the results obtained from the recent simulation [29].

Figure 7 shows potentials from the model calculations for the capillary densities used in the experimental work (Table I). The potentials are given at the capillary center along its length L. The potential labeled s refers to a single capillary. The charge of 35 fC, inserted into the capillary, is converted to absorbed charges using the curves in Fig. 6. The horizontal dashed line represents the potential barrier $T_p/q = 428$ V which cannot be overcome by ions incident with kinetic energy of $T_p = 3$ keV and charge $q = 7$. It is seen that the potentials for the lower capillary densities (3×10^6 and 5×10^6 cm^{-2}) are smaller than this barrier, whereas in the middle of the capillary, the potentials for the higher capillary densities (3×10^7 and 6×10^7 cm^{-2}) are larger than this barrier. Hence, for the high density samples the potential is dominated by the neighbors, while in case of the low density samples the potential is only slightly modified by the neighbors.

Further results are calculated for the maximum potential located in the middle of the capillary at 5 μm. In Fig. 8 the data are plotted as a function of the inserted charge which is again converted to the absorbed charge by means of Fig. 6. The figure shows a dashed dotted line at 45 V, which crosses the curves labeled d, c, b, and a near the inserted charges 2, 4, 28, and 37 fC, respectively. Looking back at Fig. 5 one can see that the transmission starts to drop at ~1, ~2, 25, and 33 fC, respectively. It is likely that at the potential of 20–40 V the deceleration of the incident beam leads to an increase of the beam divergence which in turn increases the ion absorption at the capillary wall. Thus, the present model calculation explains the much faster ion blocking within the capillaries of higher densities observed in Fig. 5.

In addition, Fig. 8 shows that the curves associated with the lower densities do not cross the potential barrier indicated by the horizontal dashed line at 428 V. This is in accordance with the experimental results that the ion blocking is small for these densities. However, the curves for the higher densities cross the potential barrier at inserted charges higher than ~15 fC. Consequently, the ion blocking is found to be significant for these densities [see Figs. 5(c) and 5(d)].

The finding that the potential exceeds the barrier at 428 V should lead to a total suppression of the ion transmission through the capillaries. In fact, a potential larger than 428 V cannot be created by 3-keV Ne^{7+} ions so that the model is not applicable in this case. Rather, Figs. 5(c) and 5(d) show a non-zero transmission even for large charge insertion. There are two reasons for this observation. First, the present model is performed with a constant current density of the incident ion beam. However, the ion beam is expected to have a density distribution described by a Gaussian function with a finite width. At the edges of the ion beam the neighbor potential is reduced so that it may become lower than the potential barrier. This would lead to a partial transmission of the ions through the capillary.

Second, as indicated by Eq. (6) in the previous subsection, the absorbed charge Q_a should be regarded as an upper limit for the charge really present within the capillaries. This absorbed charge is reduced by the transport of the charge Q_d to the capillary exits, where they can be depleted at the grounded metal layer. In fact, the electric field directed along

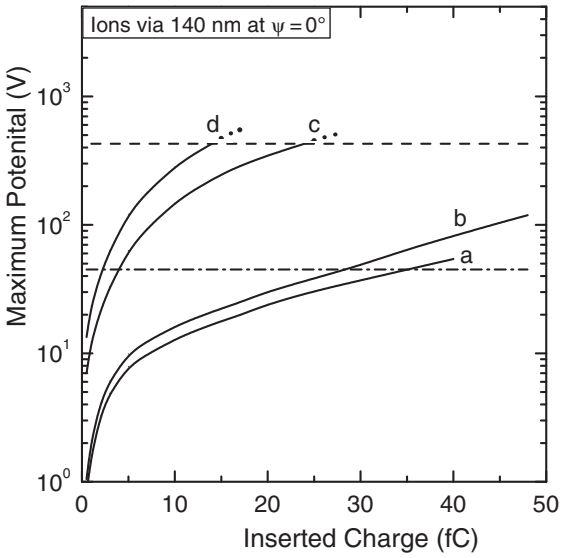

FIG. 8. Maximum potential in the middle of the capillary at 5 μm as a function of the inserted charge. Note that Fig. 6 is used to convert the inserted charge into the charge accumulated in the capillary. The curves labeled a, b, c, and d are obtained with the same capillary densities as in Fig. 7 where also the horizontal dashed line is explained. The dashed dotted line at 45 V indicates the approximate potential at which the blocking starts (see text).

the capillary axis, responsible for the charge transport, can be deduced by differentiating the corresponding curves in Fig. 7. For the higher densities the longitudinal field exceeds the value of 0.1 V/nm in the vicinity of the capillary exits. This number is close to the electrical breakthrough value for PET [28]. Hence, for the high capillary densities, the absorbed charge is transported with a high probability to the grounded metal layers. The removal of the absorbed charge becomes relatively large for the highest capillary density so that it may be understood that the blocking effect for the density of 6×10^7cm^{-2} is not much higher than that for 3×10^7 cm^{-2}.

In particular, we note that in Figs. 7 and 8 the results labeled c and d are upper limits for the potentials. On the other hand, it is expected that the curves labeled a and b, corresponding to the lower densities, represent realistic values. Altogether, the present model shows at least qualitatively that neighbor effects may be weak for capillaries of densities smaller than 10^7 cm^{-2}. However, they are important for capillary densities larger than this critical value.

V. CONCLUSIONS

The transmission of 3-keV Ne^{7+} ions through PET capillaries was measured to study blocking effects on the ion transmission for different capillary densities. The work was motivated by recent observations that PC capillaries exhibit strong ion blocking effects whereas these effects were absent for capillaries in PET [34]. Since the PC samples contained capillaries at a higher density than for the PET samples, the question arose whether the differences between PC and PET are produced by the different material properties or different densities.

The experiments clearly revealed that there is no principle difference between the PC and PET materials. Rather, the ion transmission is strongly influenced by the capillary density. For the lowest density of 3×10^6 cm^{-2} the ion transmission was found to be practically constant in agreement with the previous results obtained with PET capillaries at the same density [34]. Thus, these low-density samples show no blocking. Similarly, the blocking effect is marginal for the PET samples with a capillary density of 5×10^6 cm^{-2}.

However, drastic blocking effects on the ion transmission are observed for PET capillaries with densities higher than 10^7 cm^{-2}. Hence, the loss of transmission becomes increasingly important for a mean capillary distance of 2 μm and below (Table I). It appears that blocking becomes significant when the mean distance to adjacent capillaries is smaller than the capillary half length. The significant increase of the ion blocking can qualitatively be explained by a self-enhancing process involved in the ion absorption within the capillary. The blocking leads to an increased absorption of incident charge in the capillary interior which, in turn, increases the potential responsible for the blocking and so on. It should be added that the absorbed charge is removed by the longitudinal field determined by the derivative of the potential. When the potential or field increases, more charges are removed so that the self-enhancing process is weakened. Therefore, it may be understood that the blocking effect for the density of 6×10^7cm^{-2} is not much higher than that for 3×10^7 cm^{-2}.

In view of the strong losses observed in the ion transmission the question arises why blocking effects in PET capillaries have not been reported in earlier work. We found here that the capillary density is an important parameter, which governs ion blocking. However, it cannot be excluded that other parameters are important as well. In particular, we expect that the conductivity of the inner capillary wall plays a certain role. Further work is needed to inquire about the material properties influencing the ion transmission at high capillary densities.

Finally, in model calculations it was shown that the ion blocking may strongly be influenced by capillary neighbors. In accordance with the experimental results it was shown that for smaller capillary densities the blocking effects are relatively small. On the other hand, blocking effects are found to be significant for higher densities also in agreement with the experimental results. In fact, the calculations overestimate the blocking since the charge transport to capillary exits was not included in the model. A more realistic modeling could be performed by incorporating the neighbor capillaries into simulations of the ion guiding [25]. In particular, future studies are needed for tilt angles of a few degrees, which were not treated in the present work.

ACKNOWLEDGMENTS

We thank John Tanis for helpful comments on the manuscript. B.S. and Z.J. were supported by the Hungarian National Science Foundation OTKA (Grant No. K83886). The work was financially supported by the European Network ITSLEIF RII3-026015. Financial support for V.B. from the Volkswagen-Stiftung is acknowledged.

APPENDIX: MODELS FOR DIRECT ION TRANSMISSION

In this Appendix, we perform model calculations to analyze the direct ion transmission through a capillary, i.e., for ions that follow straight-line trajectories within a field-free capillary. As noted the experiments deal with ion transmission through capillaries with tilt angles of nearly zero degree. The direct transmission of the ion beam is strongly affected by any deviation from zero degree. Moreover, even if the tilt angle is exactly equal to zero, some intensity is absorbed within the capillary due to the fact that the ion beam slightly diverges. Here, we provide simple expressions, which allow for evaluating the ion transmission through a slightly tilted capillary involving a small beam divergence.

As noted before, the fraction of transmitted ions is given by $f_t = J_t/J_{\rm in}$, where $J_{\rm in}$ is the current, which enters into the capillary entrance and J_t is the transmitted current leaving the capillary exit. The capillary has a length L and a diameter d as shown in Fig. 9. An important quantity is the aspect ratio L/d defining the angle ϕ_a by $\tan\phi_a = d/L$.

First, we consider a beam originating from a small source area s at a distance l from the capillary (Fig. 9). The current ejected from the source into the solid angle Ω is given by $J_s = j_s\Omega$, where j_s is the current density characteristic for the source. The solid angle is obtained as $\Omega = \sigma/l^2$ where σ is the area limiting the beam. The beam entering into the capillary is limited by the capillary opening $\sigma_0 = \pi d^2/4$. The transmitted beam is determined by the overlap σ_c of two circles representing the entrance and exit opening of the capillary seen by an observer at the source point. The circles are displaced by the distance $y_m = L\tan\psi$ (Fig. 9).

Thus, the fraction of ions transmitted through the tilted capillary is obtained as $f_\psi = \sigma_c/\sigma_0$. The overlap σ_c can be determined in closed form [29] yielding an expression, which depends only on the normalized quantity $\varrho = y_m/d = \tan\psi/\tan\phi_a$. For $d \ll L$ one may set $\varrho \approx \psi/\phi_a$, which is referred to as the relative tilt angle. In Fig. 10(a) the exact results for transmitted ion fraction f_ψ is shown as a function of relative tilt angle ϱ. As expected, the effective opening is equal to unity for ion impact along the capillary axis and tends to zero when the tilt angle approaches the capillary aspect angle (for $\varrho \to 1$). It is noted that the transmission drops to 1/2 at the relative angle of $\varrho = 0.4$.

As shown previously [29], the exact transmission function can be approximated by the simple empirical expression,

$$f_\psi = (1-\varrho)^\chi\,, \tag{A1}$$

for $\varrho \leqslant 1$ and $f_\psi = 0$ elsewhere, where $\chi = 1.38$. In Fig. 10(a) the approximate results from Eq. (A1) are shown as a dashed line. The two curves coincide very well.

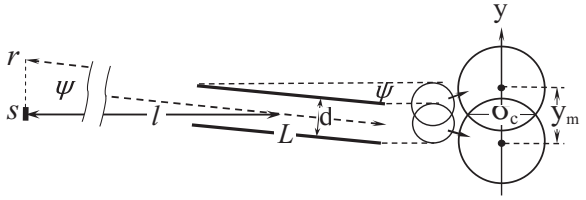

FIG. 9. Schematic drawing for the transmission of a direct beam through a slightly tilted capillary.

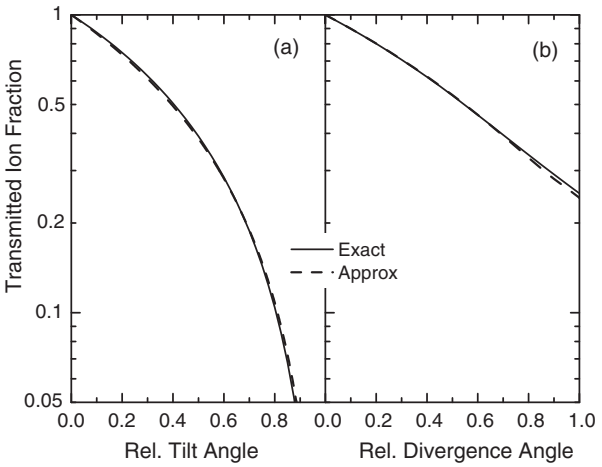

FIG. 10. Exact and approximate results for the transmitted ion fraction represented by a solid and dashed line, respectively. In (a) the transmitted ion fraction is given as a function of the relative tilt angle ϱ and in (b) the transmitted ion fraction is given as a funcrion of the relative divergence angle ϱ_d.

Next, we assume that the incident beam is absorbed within the capillary due to the divergence of the ion beam. It is characterized by the divergence angle ψ_d assuming that most of the ions are emitted within $\pm\psi_d$. Here, an untilted capillary is considered, i.e., the capillary axis lies in the center of an extended source area governed by the beam diameter ($\sim$1.3 mm). Small fractions of the ion beam are emitted from ring elements with the area $\Delta s = 2\pi\, r\, \Delta r$ where $r = l \tan\psi$ determines the tilt angle ψ (Fig. 9). As above, the relative tilt angle $\varrho \approx \psi/\phi_a$ is used. Moreover, we introduce the relative divergence angle $\varrho_d = \tan\psi_d/\tan\phi_a \approx \psi_d/\phi_a$.

The fraction f_d of ions transmitted by a diverging beam is obtained by integration over the ring elements or, equivalently, over ϱ,

$$f_d = \int_0^1 f_\psi(\varrho)\, j_s(\varrho_d,\varrho)\, \varrho\, d\varrho, \tag{A2}$$

where $\int j_s \varrho d\varrho = 1$. The upper limit of the integration is unity, since $f_\psi(\varrho) = 0$ for $\varrho > 1$ [Eq. (A1)]. The transmitted ion fraction f_d is evaluated numerically using both a Gaussian function and a step function for j_s with the full width $w_d = 2\psi_d$, which yielded similar results. The numerical results from the Gaussian function are represented by the solid line in Fig. 10(b) plotted as a function of the relative divergence angle ϱ_d.

The numerical results can be approximated by the expression,

$$f_d = \tfrac{3}{4}(1-\varrho_d)^\chi + \tfrac{1}{4}, \tag{A3}$$

for $\varrho_d \leqslant 1$ and $f_d = 1/(4\varrho_d^2)$ elsewhere. Again, $\chi = 1.38$. The results from Eq. (A3) are given as a dashed line in Fig. 10(b). The agreement between the original and approximate expressions is very good.

As an example, for the present capillary experiments $\psi_d = \pm 0.25^\circ$ and $\phi_a = \arctan(0.014) = 0.8^\circ$ so that $\varrho_d = 0.31$. For this case Eq. (A3) yields a transmission of $f_d = 0.7$ corresponding to 30% of ions absorbed within the capillary. This number is in accordance with the result of a previous simulation [29]. We recall that this value for f_d was used to normalize the fractions presented in Fig. 5.

To combine the ion transmission by the nonzero tilt and divergence angle we set

$$f_t \approx f_\psi\, f_d, \tag{A4}$$

which is a reasonable approximation for $f_t \lesssim 1$.

[1] N. Stolterfoht, J. H. Bremer, V. Hoffmann, R. Hellhammer, D. Fink, A. Petrov, and B. Sulik, Phys. Rev. Lett. **88**, 133201 (2002).

[2] N. Stolterfoht, V. Hoffmann, R. Hellhammer, D. Fink, A. Petrov, Z. D. Pešić, and B. Sulik, Nucl. Instrum. Methods Phys. Res. B **203**, 246 (2003).

[3] N. Stolterfoht, R. Hellhammer, Z. D. Pešić, V. Hoffmann, J. Bundesmann, A. Petrov, D. Fink, and B. Sulik, Vacuum **73**, 31 (2004).

[4] Y. Kanai, M. Hoshino, T. Kambara, T. Ikeda, R. Hellhammer, N. Stolterfoht, and Y. Yamazaki, Nucl. Instrum. Methods Phys. Res. B **258**, 155 (2007).

[5] R. Hellhammer, J. Bundesmann, D. Fink, and N. Stolterfoht, Nucl. Instrum. Methods Phys. Res. B **258**, 159 (2007).

[6] N. Stolterfoht, R. Hellhammer, J. Bundesmann, and D. Fink, Phys. Rev. A **77**, 032905 (2008).

[7] M. Kreller, G. Zschornak, and U. Kentsch, J. Phys: Conf. Ser. **163**, 012090 (2009).

[8] N. Stolterfoht, R. Hellhammer, Z. Juhász, B. Sulik, E. Bodewits, H. M. Dang, and R. Hoekstra, Phys. Rev. A **82**, 052902 (2010).

[9] Z. Juhász, B. Sulik, R. Rácz, S. Biri, R. J. Bereczky, K. Tőkési, Á. Köver, J. Pálinkás, and N. Stolterfoht, Phys. Rev. A **82**, 062903 (2010).

[10] D. Li, Y. Wang, Y. Zhao, G. Xiao, D. Zhao, Z. Xu, and F. Li, Nucl. Instrum. Methods Phys. Res. B **267**, 469 (2009).

[11] M. B. Sahana, P. Skog, G. Víkor, R. T. Rajendra Kumar, and R. Schuch, Phys. Rev. A **73**, 040901(R) (2006).

[12] S. Mátéfi-Tempfli, M. Mátéfi-Tempfli, L. Piraux, Z. Juhász, S. Biri, É. Fekete, I. Iván, F. Gáll, B. Sulik, G. Víkor *et al.*, Nanotechnology **17**, 3915 (2006).

[13] P. Skog, I. L. Soroka, A. Johansson, and R. Schuch, Nucl. Instrum. Methods Phys. Res. B **258**, 145 (2007).

[14] Z. Juhász, B. Sulik, S. Biri, I. Iván, K. Tőkési, É. Fekete, S. Mátéfi-Tempfli, M. Mátéfi-Tempfli, G. Víkor, E. Takács *et al.*, Nucl. Instrum. Methods Phys. Res. B **267**, 321 (2009).

[15] A. R. Milosavljević, G. Víkor, Z. D. Pešić, P. Kolarž, D. Šević, B. P. Marinković, S. Mátéfi-Tempfli, M. Mátéfi-Tempfli, and L. Piraux, Phys. Rev. A **75**, 030901(R) (2007).

[16] B. S. Dassanayake, S. Das, and J. A. Tanis, AIP Conf. Proc. **1336**, 154 (2011).

[17] S. Das, B. S. Dassanayake, M. Winkworth, J. L. Baran, N. Stolterfoht, and J. A. Tanis, Phys. Rev. A **76**, 042716 (2007).
[18] B. S. Dassanayake, D. Keerthisinghe, S. Wickramarachchi, A. Ayyad, S. Das, N. Stolterfoht, and J. A. Tanis, Nucl. Instrum. Methods Phys. Res. B **298**, 1 (2013).
[19] G. P. Pokhil, K. A. Vokhmyanina, L. A. Zhilyakov, T. Ikeda, Y. Kanai, Y. Iwai, T. M. Kojima, and Y. Yamazaki, Bull. Russian Acad. Sci. Phys. **72**, 638 (2008).
[20] R. Bereczky, G. Kowarik, F. Aumayr, and K. Tőkési, Nucl. Instrum. Methods Phys. Res. B **267**, 317 (2009).
[21] G. Kowarik, R. J. Bereczky, F. Aumayr, and K. Tőkési, Nucl. Instrum. Methods Phys. Res. B **267**, 2277 (2009).
[22] T. Ikeda, T. M. Kojima, Y. Iwai, Y. Kanai, T. Kambara, T. Nebiki, T. Narusawa, and Y. Yamazaki, J. Phys: Conf. Ser. **58**, 68 (2007).
[23] A. Cassimi, T. Muranaka, L. Maunoury, H. Lebius, B. Manil, B. A. Huber, T. Ikeda, Y. Kanai, T. M. Kojima, Y. Iwai *et al.*, Int. J. Nanotechnol. **5**, 809 (2008).
[24] E. Gruber, G. Kowarik, F. Ladening, J. P. Waclawek, F. Aumayr, R. J. Bereczky, K. Tőkési, P. Gunacker, T. Schweigler, C. Lemell *et al.*, Phys. Rev. A **86**, 062901 (2012).
[25] K. Schiessl, W. Palfinger, K. Tőkési, H. Nowotny, C. Lemell, and J. Burgdörfer, Phys. Rev. A **72**, 062902 (2005).
[26] K. Schiessl, W. Palfinger, K. Tőkési, H. Nowotny, C. Lemell, and J. Burgdörfer, Nucl. Instrum. Methods Phys. Res. B **258**, 150 (2007).
[27] K. Schiessl, K. Tőkési, B. Solleder, C. Lemell, and J. Burgdörfer, Phys. Rev. Lett. **102**, 163201 (2009).
[28] N. Stolterfoht, Phys. Rev. A **87**, 012902 (2013).
[29] N. Stolterfoht, Phys. Rev. A **87**, 032901 (2013).
[30] P. Skog, H. Q. Zhang, and R. Schuch, Phys. Rev. Lett. **101**, 223202 (2008).
[31] Y. Kanai, M. Hoshino, T. Kambara, T. Ikeda, R. Hellhammer, N. Stolterfoht, and Y. Yamazaki, J. Phys: Conf. Ser. **194**, 012068 (2009).
[32] N. Stolterfoht, R. Hellhammer, D. Fink, B. Sulik, Z. Juhász, E. Bodewits, H. M. Dang, and R. Hoekstra, Phys. Rev. A **79**, 022901 (2009).
[33] H.-Q. Zhang, P. Skog, and R. Schuch, Phys. Rev. A **82**, 052901 (2010).
[34] N. Stolterfoht, R. Hellhammer, B. Sulik, Z. Juhász, V. Bayer, C. Trautmann, E. Bodewits, and R. Hoekstra, Phys. Rev. A **83**, 062901 (2011).
[35] M. Unipan, A. Robin, D. F. A. Winters, R. Morgenstern, and R. Hoekstra, Phys. Rev. A **74**, 062901 (2006).
[36] G. Pépy, P. Boeseck, A. Kuklin, E. Manceau, B. Schiedt, Z. Siwy, M. Toulemonde, and C. Trautmann, J. Appl. Crystallogr. **40**, s388 (2007).
[37] N. Stolterfoht, R. Hellhammer, Z. Juhász, B. Sulik, V. Bayer, C. Trautmann, E. Bodewits, A. J. de Nijs, H. M. Dang, and R. Hoekstra, Phys. Rev. A **79**, 042902 (2009).